Carbon Letters (2023) 33:823–832
https://doi.org/10.1007/s42823-023-00463-w

Online ISSN 2233-4998
Print ISSN 1976-4251

ORIGINAL ARTICLE

An hydrogen adsorption study on graphene-based surfaces with core–shell type catalysts

Emmanuel Vallejo[1]

Received: 16 September 2022 / Revised: 6 January 2023 / Accepted: 9 January 2023 / Published online: 20 January 2023

Abstract

An hydrogen adsorption study on graphene-based surfaces consisting of nitrogen-doped graphene and core–shell type catalysts of initially Pd_{13}, Pt_{13}, $PdPt_{12}$ and $PtPd_{12}$ core–shells, is presented in this work. Density functional theory results indicate correlation between charge transfer and structural properties, hydrogen adsorption energies, magnetic behavior and electronic properties. Reduction of hydrogen, together with higher values of charge transfer was observed for high hydrogen dissociation, compared to the case of non-hydrogen dissociation. In some cases, these values may be almost an order of magnitude larger than that of non-hydrogen dissociation. Hydrogen dissociation is also related to oxidation of the surface and correlates with a non-core shell-type structure, high adsorption energies and low magnetic moments, in general. Besides, core shell-type structure dramatically changes the magnetic and electronic properties of charge transfer. The results obtained in this work may provide important information for storing hydrogen.

Keywords Modeling of materials · Magnetic materials · Electronic materials · Core–shell-type catalysts

1 Introduction

Hydrogen adsorption involves molecular hydrogen activation and dissociation that are important for storing hydrogen as vehicle fuel [1, 2] and also for fuel cell applications. Hydrogen storage requires high volumetric and gravimetric densities, low molecular hydrogen sorption temperature, fast reaction kinetics and effective reversibility [1]. Several methods to store energy require low temperatures, high pressures, or chemical compounds to release hydrogen on demand. Correspondingly, molecular dynamic simulations were used to study the effect of pressure and temperature on adsorption energy and gravimetric density [3–5].

The nature of the support and catalyst has important influence on catalytic performance, in terms of hydrogen adsorption, dissociation and desorption [6]. Molecular hydrogen can be dissociated by any metal adsorbed on any surface to form dihydride systems. Transition metal nanoparticles represent the most promising catalysts for hydrogen activation, dissociation and consequently for adsorption. For example, Pt and Pd catalysts can be used for a wide range of reactions such as hydrogenation, dehydrogenation and dehalogenation. The dissociative chemisorption of hydrogen on Pt and Pd clusters is easy and involves strong bonds between the Pt and Pd clusters and the hydrogen [6]. Binding energy between Pt clusters and H atoms is 56 kcal/mol and 74 kcal/mol, at full and zero hydrogen coverage respectively [7]. Significantly, dissociative chemisorption of molecular hydrogen is barrierless for carbon supported and Pt_4 clusters [8, 9]. In the case of Pd dissociative chemisorption, barriers of molecular hydrogen are dependent on cluster size [6]: For example barriers of molecular hydrogen of ~ 0, ~ 0, 10.6, 6.0, 6.9, 2.9, and 0.7 kcal/mol can be observed in Pd_2, Pd_3, Pd_4, Pd_5, Pd_6, Pd_9 and Pd_{13} clusters, respectively [2, 10–12].

In addition to catalysts, the support is important because it conditions the active site in reactivity [6]. Supports are critical for the efficiency and stability of catalytic systems and supports may even function as catalysts themselves [6]. The support has influence on catalytic properties because of charge transfer, structure of the metal nanoparticle and the specific active sites at the metal-support boundary [6]. Consequently, different effects can be considered, i. e. electronic, geometric, spillover and confinement [6]. The support can be based on carbon or it can be doped with for

✉ Emmanuel Vallejo
emmanuel_vallejo@uaeh.edu.mx

[1] Escuela Superior de Apan, Universidad Autónoma del Estado de Hidalgo, Carretera Apan-Calpulalpan Km. 8, Col. Chimalpa, 43920 Apan, Hidalgo, Mexico

example nitrogen, to alter its properties. Nitrogen doped carbon support has claimed attention due to the fact that nitrogen doping is able to modify the properties of carbon support systems for various applications of interest. Some examples include super capacitor applications and electrocatalysts for the Oxygen Reduction Reaction. The pyridinic nitrogen system in particular exhibits experimentally higher chemical reactivity than pyrrolic or graphitic and traps better atoms, such as Mg, Al, Ca, Ti, Mn, and Fe.

Furthermore, when doping of the support with nitrogen or boron is undertaken, this also affects the Pd–H bonding energy [13–18]. An energy barrier of 60 kcal/mol [10] was found to migrate atomic hydrogen from the a Pd_{13} cluster to the clean graphene support. The former value diminishes to 48 kcal/mol, if the cluster is saturated with 10 hydrides. Pd clusters adsorbed on graphene with vacancies have been studied for hydrogen storage. Pristine graphene with vacancies alters the electronic structure of the catalysts (transition metal clusters), as a result of charge transfer. In the same way vacancies affect binding energy [19]. Charge transfer from the metal to the support (graphene) is induced, when vacancies or nitrogen atoms are present and control for example, O_2 or CO adsorption [6]. Charge transfer may be very important for photo, electro and thermal catalysis [6]. Charge transfer, typical of a covalent chemical bond with partial ionic character was observed to occur as a consequence of the interaction between pyridine N and Pd [20]. The influence of charge transfer on dihydride dissociation requires investigation. For example, spontaneous dissociation of H_2 was reported for small Pt clusters [21].

Another important phenomenon involved in hydrogen adsorption and dissociation is hydrogen spillover, defined as the transport of species to another surface, which does not adsorb or form these species under the same conditions [6, 22]. Hydrogen spillover consists of several steps: (1) molecular hydrogen is activated and dissociated on a catalyst in contact with the support, (2) subsequently, migration from the catalyst to the support of H species is expected [6]. Furthermore, spillover involves transport phenomena of atoms other than hydrogen, such as O, CO [23] or S [24]. Spillover is not favorable for a defect-free surface of a carbon support [8, 25], but it is possible if the carbon support presents defects or when it is doped [1]. Theoretical studies [25, 26], focused on calculating energy barriers (2.7 eV = 62.26 kcal/mol [26] and 2.6 eV = 59.96 kcal/mol [25]) for hydrogen migration from the Pt_4 cluster to the carbon surface were proposed. In the case of Pd_6 and Pd_{13} clusters supported on graphene barriers of 2.7 eV were calculated [10]. These results suggest that hydrogen migration is very difficult and that under normal conditions, spill-over would not occur [1]. In the case of Pd_{13} and Pd_6 clusters anchored on pristine graphene [10], molecular dynamics were used and not a single dissociation was present in the hydrogen saturated clusters. Furthermore, to date, there is no general consensus that satisfactorily explains spill-over.

We recently studied the interplay between N-graphene defects and small Pd (Pd_n, $n = 1 - 4$) clusters for enhanced hydrogen storage, via a spill-over mechanism [1]. We found migration energy barriers of 0.5–0.8 eV (11.53–18.45 kcal/mol), suggesting that migration from the Pd-clusters to the N-graphene support may occur spontaneously at room temperature [1].

The main objective of this article is to study hydrogen adsorption on graphene-based surfaces with core–shell type catalysts. Besides, the objetive is to study charge transfer and how charge transfer relates to structural properties, hydrogen adsorption energies, magnetic behavior and electronic properties of a particular nitrogen-doped graphene surface. Notably, the surface will be coupled to various catalysts, initially composed of Pd_{13}, Pt_{13}, $PdPt_{12}$ and $PtPd_{12}$ core–shell structures.

The paper is organized as follows. In Sect. 2 a brief description of the methodology is given. In Sect. 3, structural parameters, charge transfer, adsorption energies, magnetic and electronic properties are discussed. Finally, the results are summarized in Sect. 4.

2 Computational methods

In this work, Density Functional Theory (DFT) was implemented with the Vienna Ab-initio Simulation Package (VASP) [27, 28]. In the same way, the Projector Augmented Wave (PAW) method [29, 30] and the GGA functionals were also utilized. Additionally the exchange correlation form according to the Perdew–Burke–Ernzerhof (PBE) [31] exchange correlation was also considered.

DFT together with GGA and PBE was also considered to study hydrogen storage using small Pd-clusters and N-graphene defects in our previous work [1]. In reference [1] GGA and PBE functionals were used to calculate barrier energies and other physical properties. The former functionals were compared with the HSE06 hybrid functional to verify the accuracy of the GGA and PBE functionals. It was found for example a difference < 0.2 eV in barrier energies between GGA and HSE06 functionals [1].

In this work chemically bound hydrogen molecules is of interest and is the reason why van der Waals interactions were not considered. Furthermore, Monkhorst-Pack sampling and a value of 500 eV for the energy cutoff were used. In all our calculations the $1s^1$, $2s^22p^2$, $2s^22p^3$, $5s^14d^9$ and $6s^15d^9$ configurations were considered as valence electrons for H, C, N, Pd and Pt atoms respectively. Finally, an exhausted analysis was carefully performed to ensure energy convergence of $\Delta E < 0.001$ eV/atom. The former energy convergence was achieved using $(3 \times 3 \times 1)$

k-points and an energy cutoff of 500 eV. Electronic charge density difference ($< 1 \times 10^{-4}$) and an ionic force convergence criterion ($< 2 \times 10^{-2}$ eV/Å) were used. In this paper a slab model composed of a periodic hexagonal unit cell ($a = b = 12.20$ Å and $c = 16.00$ Å) of C_{50} carbon ions was considered. The magnitude of c was used as the vacuum space to prevent interactions between slabs. Two vacancies (V) were introduced in the unit cell and 4 N ions replaced 4 C ones in a pyridinic way to change the properties of graphene. The unit cell is composed of a pyridinic $C_{44}N_4V_2 \equiv N_4V_2$ system. The slab model proposed and the nitrogen content is comparable with experimental results as it will be discussed in Sect. 3. Several clusters Pd(Pt)-based and hydrogen ions were also introduced in the former model to study hydrogen adsorption.

3 Results and discussions

The system studied in this paper initially entails a N_4V_2 pyridinic substrate (nitrogen content of 8.3%) and an ensemble of Pd-Pd_{12}, Pt-Pt_{12}, Pd-Pt_{12} and Pt-Pd_{12} core–shells as catalysts. Notably, the nitrogen content in our model is comparable to experimental results. For example, the experimental nitrogen content for a pyridinic and graphitic substrate synthesized using the deposition-precipitation method [32] was 5.7%, 8.6%, and 11.3%. Likewise, the nitrogen content for pyridinic, pyrrolic and graphitic defects was 7% in a N-doped graphene via nitrogen plasma treatment of hydrogen exfoliated graphene [33]. Formation energies for different nitrogen-doped graphene defects were calculated previously [34]. Consequently, it was suggested that N_4V_2 pyridinic defect will predominate in experimental conditions, over other N_xV_y ones. This is the main reason for considering the N_4V_2 (nitrogen content of 8.3%) as the substrate.

Additionally, transition metal nanoparticles like Pt or Pd are the most promising catalysts for hydrogen adsorption and they will be considered as the main components in our catalysts. In this work, the hydrogen molecule was initially placed at different orientations and on top of the catalysts. The results of certain structures, selected according to their lowest energies are presented in Fig. 1. Part of our figures were made using the XCrySDen software [35]. The physical properties vary depending on the position of the hydrogens around the catalyst, as apparent in the Supporting Information (SI) (Figure $\mathcal{S}1$ in SI). System number 20 was used for the former case, where the hydrogen molecule was placed very close to the surface. From a qualitative point of view, the results in terms of charge transfer and its correlation with other properties remain. Depending on the position of the hydrogen molecule on the cluster, two states were to be expected; one activated and the other dissociated; the dissociated state manifests higher hydrogen adsorption energies, large hydrogen-hydrogen distances and low magnetic moments [1, 13, 17, 36]. An exhaustive study concerning the influence incurred by the position of hydrogens around the catalysts will be the subject of another study.

Hydrogen adsorption energies (ΔE) on optimized structures (OS) were calculated as $\Delta E = E_{OS+2H} - E_{OS} - E_{H_2}$ [1, 37]. E_{OS+2H} is the total energy of the optimized structure

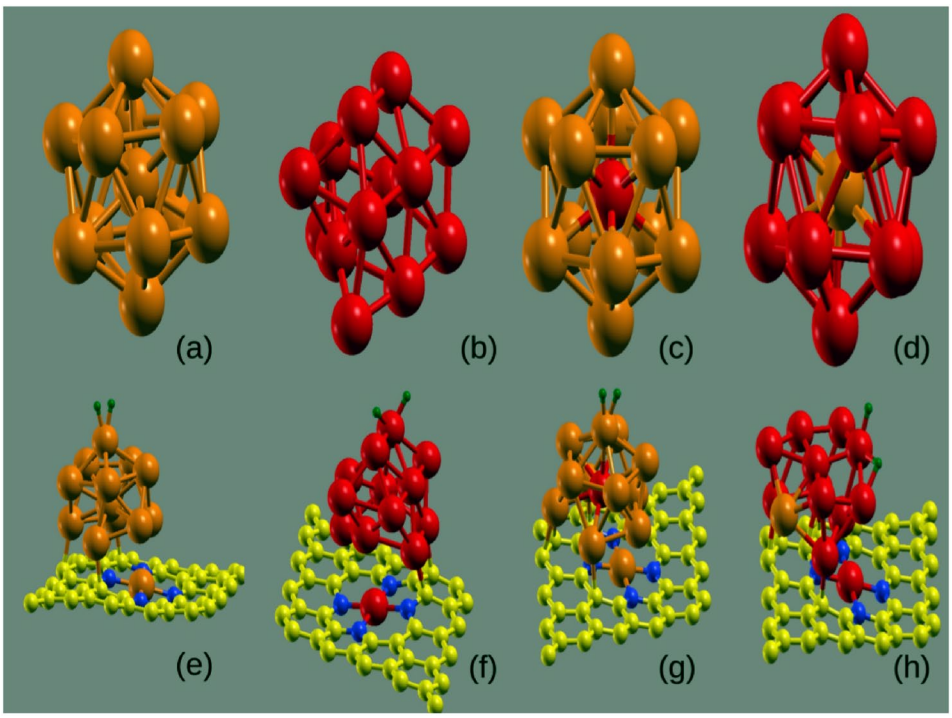

Fig. 1 Selected structural representations. System numbers (SN) in accord with Tables 1 and 2 are also indicated. **a** $PdPd_{12}$ SN = 3, **b** $Pt_{13}(1)$ SN = 4, **c** $PtPd_{12}$ SN = 6, **d** $PdPt_{12}(1)$ SN = 7, **e** PdN_4V_2 -$PdPd_{11}$-2H SN = 18, **f** PtN_4V_2 -$Pt_{12}(1)$-2H SN = 19, **g** PdN_4V_2 -$PtPd_{11}$-2H SN = 20 and **h** PtN_4V_2-$PdPt_{11}(1)$-2H SN = 21. Yellow, blue, brown, red and green colors are asigned to carbon, nitrogen, palladium, platinum and hydrogen ions respectively

Table 1 Hydrogen-hydrogen d_{H-H} distance in Å and a core–shell type are presented in this table

System number	System	d_{H-H}	Core–shell type
1	H_2	0.75	
2	N_4V_2		
3	Pd_{13}		Pd-Pd_{12}
3-v	Pd_{13}(2)		Not
4	Pt_{13}(1)		Not
5	Pt_{13}(2)		Pt-Pt_{12}
6	$PtPd_{12}$		Pt-Pd_{12}
7	$PdPt_{12}$(1)		Pd-Pt_{12}
7-v	$PdPt_{12}$(2)		Not
8	N_4V_2+2H	0.75	
9	Pd_{13}+2H	0.87	Pd-Pd_{12}
10	Pt_{13}(1)+2H	1.86 (∗)	Not
11	Pt_{13}(2)+2H	1.82 (∗)	Pt-Pt_{12}
12	$PtPd_{12}$+2H	0.86	Pt-Pd_{12}
13	$PdPt_{12}$(1)+2H	1.84 (∗)	Pd-Pt_{12}
13-v	$PdPt_{12}$(2)+2H	2.23 (∗)	Not

The symbol (∗) indicates hydrogen dissociation according to reference [10]

Table 2 Substrate vertical mean absolute deviation Z_{MAD} in Å, hydrogen-hydrogen d_{H-H} distance in Å and a core–shell type are presented in this table

System number	System	Z_{MAD}	d_{H-H}	Core–shell type
14	PdN_4V_2-$PdPd_{11}$	0.22		Pd-Pd_{11}
15	PtN_4V_2-Pt_{12}(1)	0.23		Not
16	PdN_4V_2-$PtPd_{11}$	0.22		Pt-Pd_{11}
17	PtN_4V_2-$PdPt_{11}$(1)	0.24		Not
18	PdN_4V_2-$PdPd_{11}$+2H	0.21	0.88	Pd-Pd_{11}
19	PtN_4V_2-Pt_{12}(1)+2H	0.23	2.14 (∗)	Not
20	PdN_4V_2-$PtPd_{11}$+2H	0.22	0.89	Pt-Pd_{11}
21	PtN_4V_2-$PdPt_{11}$(1)+2H	0.25	2.28 (∗)	Not

The symbol (∗) indicates hydrogen dissociation according to reference [10]

following hydrogen adsorption. E_{OS} and E_{H_2} represent total energies of the optimized structures and molecular hydrogen, respectively. In this case $\Delta E < 0$ implies hydrogen adsorption. This energy may also imply activation and dissociation hydrogen energy.

Structural parameters that could include a hydrogen-hydrogen distance, a substrate vertical mean absolute deviation as used in reference [38] and a core shell-type structure indicator are presented in Tables 1 and 2, for selected structures, characterized by a system number (SN). Additional structural parameters can be found in Tables $\mathcal{S}1$ and $\mathcal{S}2$ in supporting information. A structure, not of the core shell-type, is the one where the core is not observed within the shell and a cluster is simply formed, see for example Fig. 1h. All these structures are discussed after optimization. Tables 3 and 4 present a Bader analysis to study charge transfer. Likewise, adsorption energies and magnetic moments are presented in Tables 5 and 6.

Table 3 Bader analysis, $(2H)^{\pm y}$ (± y) hydrogen charge transfer and hydrogen dissociation is presented in this table

System number	Bader analysis	±y	Hydrogen dissociation
8	$C_{44}{}^{4.5}N_4{}^{-4.5}H_2{}^{0.00}$	+ 0.00	Not
9	$Pd^{0.13}(Pd_{12})^{-0.14}(2H)^{0.01}$	+ 0.01	Not
12	$Pt^{0.03}(Pd_{12})^{-0.03}(2H)^{+0.00}$	+ 0.00	Not
14	$(PdN_4V_2)^{-0.09}Pd^{0.11}(Pd_{11})^{-0.02}$		
16	$(PdN_4V_2)^{-0.11}Pt^{-0.02}(Pd_{11})^{0.13}$		
18	$(PdN_4V_2)^{-0.06}Pd^{0.08}(Pd_{11})^{-0.02}(2H)^{0.00}$	+ 0.00	Not
20	$(PdN_4V_2)^{-0.08}Pt^{-0.05}(Pd_{11})^{0.13}(2H)^{-0.00}$	− 0.00	Not

Table 4 Bader analysis, $(2H)^{\pm y}$ (± y) hydrogen charge transfer and hydrogen dissociation is presented in this table

System number	Bader analysis	±y	Hydrogen dissociation
10	$(Pt_{13}(1))^{-0.04}(2H)^{+0.04}$	+ 0.04	Yes
11	$Pt^{+0.24}(Pt_{12}(2))^{-0.29}(2H)^{+0.05}$	+ 0.05	Yes
13	$Pd^{0.28}(Pt_{12}(1))^{-0.33}(2H)^{0.05}$	+ 0.05	Yes
13-v	$(PdPt_{12}(2))^{0.03}(2H)^{-0.03}$	− 0.03	Yes
15	$(PtN_4V_2)^{+0.10}(Pt_{12}(1))^{-0.10}$		
17	$(PtN_4V_2)^{+0.10}(PdPt_{11}(1))^{-0.10}$		
19	$(PtN_4V_2)^{+0.08}(Pt_{12}(1))^{-0.03}(2H)^{-0.05}$	− 0.05	Yes
21	$(PtN_4V_2)^{+0.03}(PdPt_{11}(1))^{0.06}(2H)^{-0.09}$	− 0.09	Yes

3.1 Structural parameters

Structural characterization is presented in this section. Initially N_4V_2 pyridinic substrate, together with some Pd-Pd_{12}, Pt-Pt_{12}, Pd-Pt_{12} and Pt-Pd_{12} core shell-type structures were considered. After structural optimization several structures in the gas phase are presented in Table 1. Furthermore, in Table 2, some structures will be discussed, after interaction with N_4V_2 pyridinic substrate and after hydrogen adsorption. Structural representations of selected systems are presented in Fig. 1.

Specific parameters such as H–H distance d_{H-H} are presented in Tables 1 and 2 (other typical A-B ion distances d_{A-B} can be observed in Tables $\mathcal{S}1$ and $\mathcal{S}2$ in SI).

Table 5 Hydrogen adsorption energies ΔE in eV/Kcal mol^{-1}, magnetic moment m in μ_B, hydrogen dissociation and (± y) hydrogen charge transfer, are presented in this table

System number	System	ΔE	m	Hydrogen dissociation	±y
8	N_4V_2+2H	− 0.03/− 0.69	0.00	Not	+ 0.00
9	Pd_{13}+2H	− 0.63/− 14.63	7.18	Not	+ 0.01
10	$Pt_{13}(1)$+2H	− 1.64/− 37.77	4.06	Yes	+ 0.04
11	$Pt_{13}(2)$+2H	− 1.36/− 31.36	5.62	Yes	+ 0.05
12	$PtPd_{12}$+2H	− 0.64/− 14.83	7.91	Not	+0.00
13	$PdPt_{12}(1)$+2H	− 1.25/− 28.92	4.76	Yes	+ 0.05
13-v	$PdPt_{12}(2)$+2H	− 1.64/− 37.73	3.31	Yes	− 0.03
18	PdN_4V_2-$PdPd_{11}$+2H	− 0.74/− 17.04	4.78	Not	+ 0.00
19	PtN_4V_2-$Pt_{12}(1)$+2H	− 1.74/− 40.15	2.27	Yes	− 0.05
20	PdN_4V_2-$PtPd_{11}$+2H	− 0.87/− 20.13	5.06	Not	− 0.00
21	PtN_4V_2-$PdPt_{11}(1)$+2H	− 1.40/− 32.28	0.19	Yes	− 0.09

Table 6 Magnetic moment m in μ_B is presented in this table

System number	System	m
1	H_2	0.00
2	N_4V_2	0.00
3	Pd_{13}	8.17
3-v	$Pd_{13}(2)$	8.11
4	$Pt_{13}(1)$	3.40
5	$Pt_{13}(2)$	4.67
6	$PtPd_{12}$	8.07
7	$PdPt_{12}(1)$	3.81
7-v	$PdPt_{12}(2)$	4.40
14	PdN_4V_2-$PdPd_{11}$	4.31
15	PtN_4V_2-$Pt_{12}(1)$	3.70
16	PdN_4V_2-$PtPd_{11}$	5.30
17	PtN_4V_2-$PdPt_{11}(1)$	3.63

Specific H–H distance is important, when describing molecular hydrogen dissociation. A molecular hydrogen dissociation may be considered when the hydrogen internuclear distance exceeds 1.6 Å [10]. In Tables 1 and 2, hydrogen dissociation is indicated by the (∗) symbol. The greatest dissociation correlates directly with a non-core shell-type structure, see for example Table 1 and 2. The former hydrogen dissociation condition (1.6Å) is almost twice the hydrogen-hydrogen distance for the hydrogen molecule in the gas phase of 0.75Å, see Table 1. This distance is similar to previously reported results for 0.75 Å [37, 39, 40]. Our results can be compared to those obtained for hydrogen adsorption in reference [37]. A hydrogen-hydrogen distance of $d_{H-H} = 0.81 - 0.84$ Å was observed in a typical Kubas configuration of a system formed out of SiC substrate with one Pd-atom as catalyst. This result can be compared to the distance of our system number 18 of 0.88 Å, see Table 2. In our selected system, a PdN_4V_2-$PdPd_{11}$ structure interacts with a molecular hydrogen. The distance in our system is a little bit longer than that found in reference [37], due to the effect of our substrate.

Generally, other structures with lower energies than the corresponding Pt-Pt and Pd-Pt core–shell structures were found. For example the system number 4 ($Pt_{13}(1)$) in Table 1 that can be observed in Fig. 1b. For system number 19, see Fig 1f and system number 21 can be observed in Fig 1h.

After optimization, the initial Pt-core ion and the Pd-core were found outside the cluster in the Pt-shell, forming a straight forward cluster, see Fig 1b, f, h. The former phenomenon is comparable with the inversion process found in reference [41]. Notably, there was an apparent structural transformation of the SN = 7 core–shell structure (Fig 1d) to a non-core, shell-type structure (SN = 17 or 21 see Table 2) that was surface-mediated.

In the gas phase, for the core–shell structures (SN = 3,6 and 7), the average distance between the core ion and the ions forming the shell is ~ 2.61–2.64 Å. Additionally, average distance between first neighboring ions that form the shell is ~ 2.74–2.78 Å. Apparently, when our selected gas phase structures (SN = 3,4,6 and 7 in Table 1) interact with the N_4V_2 surface, see Figure 1e–h in main text and Figure $\mathcal{S}2$ in SI, one transition metal ion of the catalyst typically becomes detached from the cluster forming the substrate. The results from magnetic and electronic properties confirm this premise. This behavior is similar to that proposed by Cardozo-Mata et al. [34]. The transition metal adsorbed on the N_4V_2 surface changes the electronic and magnetic properties of the N_4V_2 substrate, as initially considered. In this case, a better nomenclature for the substrate can be proposed as $Pd(Pt)N_4V_2$ see Table 2, being Pd(Pt) the transition metal ion adsorbed on the N_4V_2 substrate that was initially considered.

Generally it seems that the effect of the presence of the substrate on core–shell systems is to increase the average distance between the core ion and the ions that form the shell

and likewise to decrease the first neighbor's average distance between the ions that form the shell.

A vertical mean absolute deviation $Z_{MAD} = \frac{1}{N}\sum_{i=1}^{N} |z_i - \langle z \rangle|$ [38] was also calculated on (Pd,Pt)N_4V_2 substrate, see Table 2. As reference, the graphene is perfectly flat, meaning that the corresponding vertical deformation is $Z_{MAD} = 0$. Vertical deformation increases to $Z_{MAD} = 0.13$ Å for N_4V_2 system. The characteristic graphene sp^2 symmetry is distorted because of the vacancies and a little contribution from sp^3 is the reason for the increase of Z_{MAD}. The former vertical deformation relaxes somewhat when molecular hydrogen is introduced, even if there is a physical interaction (adsorption energy of 30 meV) between the substrate and the molecular hydrogen. In this case $Z_{MAD} = 0.12$ Å.

Vertical deformation increases when catalytic clusters are introduced to the system, see Table 2, for example $Z_{MAD} = 0.21 - 0.22$ Å, when the catalysts mainly consist of Pd ions and 0.23–0.25 Å for Pt ions, see Table 2. Vertical deformation directly correlates with the greatest dissociation.

3.2 Charge transfer

Bader analysis was used to study charge transfer. Charge transfer was calculated as valence electrons (described in the computational methods) minus Bader electrons. The representation of charge transfer for example for the carbon ion will be $C^{\pm x}$ or $\pm xe^-$, being ± x charge transfer. In the case of 2 hydrogens, $(2H)^{\pm y}$ will be the hydrogen charge transfer presented in Tables 3 and 4. Bader analysis of this section can be observed in Tables 3 and 4. A positive value for charge transfer indicates oxidation and a negative one indicates reduction of the system. It is generally apparent that there is a correlation between non-hydrogen dissociation and a very low hydrogen charge transfer Table 3. In this case, we have the SN = 8 ($(2H)^{0.00}$), SN = 9 ($(2H)^{+0.01}$) , SN = 12 ($(2H)^{+0.00}$), SN = 18 ($(2H)^{+0.00}$) and SN = 20 ($(2H)^{-0.00}$) of Table 3. Contrarily, the highest values for hydrogen dissociation were obtained when the hydrogens (2H) were reduced, as in SN = 13-v ($(2H)^{-0.03}$), system number 19 ($(2H)^{-0.05}$) and 21 ($(2H)^{-0.09}$) of Table 4.

3.2.1 Systems without hydrogen dissociation

System number 8 in Table 3 does not present dissociation of hydrogen, Table 3. The hydrogen-hydrogen distance (0.75Å) is characteristic of molecular hydrogen in the gas phase. The former agrees with physical adsorption (−0.03 eV) and correspondingly, this agrees with very low hydrogen charge transfer ($0.00e^-$). SN = 8 results from molecular hydrogen and graphene substrate doped with nitrogen (GNS≡N_4V_2) denoted as system number 2. SN = 2 presents charge transfer from the carbon ions to the nitrogen ions: $\sim 4.5e^-$ $(C_{44})^{4.5}(N_4)^{-4.5}$, Table 3. This is to be expected because the electronegativity of nitrogen exceeds the electronegativity of carbon.

System number 9 in Table 3 does not present hydrogen dissociation and is made up of the Pd-Pd_{12} core–shell system (system number 3) and two hydrogens. The SN = 9 presents charge transfer from the Pd-core ($0.13e^-$) and the hydrogen ions ($0.01e^-$) to the Pd_{12}-shell ($-0.14e^-$), Table 3. This implies a reduction in the Pd_{12}-shell. At the moment when the core–shell of system number 3 is incorporated into GNS, system number 14 of Table 3 is obtained. Charge transfer of $0.11e^-$ from the Pd-core to the Pd_{11}-shell ($-0.02e^-$) and charge transfer to the substrate ($-0.09e^-$) is calculated, Table 3. The same qualitative behavior is observed when the former system adsorbs hydrogen (system number 18 in Table 3), in this case the charge transfer from the Pd-core decreases slightly to $0.08e^-$ and the charge transfer to the Pd_{11}-shell remains at $-0.02e^-$, Table 3. No charge transfer to hydrogens is apparent, Table 3. The effect of hydrogen adsorption on charge transfer properties in the former case acts to lower the charge transfer value from the core to the substrate, meaning that the hydrogens indirectly decrease the reduction at the surface.

Another system that does not present hydrogen dissociation is system number 12 in Table 3. This system consists of the Pt-Pd_{12} core–shell system (SN = 6) and two hydrogens. The SN = 12 presents qualitatively similar charge transfer behavior to that presented by system number 9. This implies charge transfer from the Pt-core ($0.03e^-$) to the Pd_{12}-shell ($-0.03e^-$). Charge transfer of the hydrogen ions has a very low value of $+0.00e^-$, Table 3. The result of changing the palladium core for platinum results in a less reduced Pd_{12}-shell. This may occur because the electronegativity of platinum exceeds that of palladium.

In contrast, if the core–shell (Pt-Pd_{12}) of system number 6 is incorporated into to GNS, system number 16 is obtained. Similarly, when SN = 16 adsorbs hydrogen system number 20 is obtained.

In the first case, (SN = 16) charge transfer from the Pd_{11}-shell ($0.13e^-$) to the Pt-core ($-0.02e^-$) and charge transfer to the substrate ($-0.11e^-$) is obtained, Table 3. This implies a reduction of the substrate. Similar behavior occurs after hydrogen adsorption (SN = 20), Table 3. In the former case, no charge transfer to hydrogens is apparent and the oxidized state of Pd_{11}-shell ($0.13e^-$) remains after hydrogen adsorption, Table 3. In this case, the effect of hydrogen adsorption is to decrease the reduction of PdN_4V_2 at the surface from $-0.11e^-$ to $-0.08e^-$. In very general terms, the non-dissociation of hydrogen is related to core–shell structure, very low charge transfer of hydrogens and to the reduction of the PdN_4V_2 surface. Likewise,

a very different qualitative behavior for charge transfer is observed, when the core of the core–shell structure is changed from Pd to Pt; in the second case, the electronegativity of Pt causes charge transfer to occur from the Pd_{11} -shell to the surface and to the Pt-core, Table 3.

3.2.2 Systems that manifest hydrogen dissociation

Unlike systems that do not present hydrogen dissociation, hydrogen dissociation is closely correlated with the oxidation of the PtN_4V_2 surface, and with a non-core shell-type structure of the systems, Table 4. Reduction at the surface is very important for hydrogen storage by means of the spillover mechanism. For non-reducible supports, it is not clear whether hydrogen spillover takes place [42]. In our systems, non-reduction at the surface is related to hydrogen dissociation.

The first system that presents hydrogen dissociation is system number 10 in Table 4. This system consists of the $Pt_{13}(1)$ cluster (SN = 4) and two hydrogens. The former system presents charge transfer from the hydrogens ($0.04e^-$) to the cluster, Table 4. In this case, the hydrogens collectively acquire an oxidized state. The former system can be compared to SN = 11 in Table 4. The SN = 11 is a Pt-$Pt_{12}(2)$ core shell-type structure and similar qualitative charge transfer behavior was found to that of the previous case, Table 4. In this case, charge transfer from the hydrogens ($+0.05e^-$) to the core–shell was obtained, Table 4. The interaction of the SN = 4 with GNS (SN = 15 in Table 4) produces oxidation of the $(PtN_4V_2)^{+0.10}$ surface and reduction ($-0.10e^-$) of the $Pt_{12}(1)$ cluster, Table 4. The interaction of the former system with hydrogen (system number 19) diminishes both surface ($+0.08e^-$) and $Pt_{12}(1)$ cluster ($-0.03e^-$) charge transfer values, in addition to reducing the hydrogens ($-0.05e^-$), Table 4. The effect of hydrogens in the former system is to decrease oxidation of the surface, as well as to decrease the reduction of the $Pt_{12}(1)$ cluster.

Two other systems that exhibit hydrogen dissociation are those of SN = 13 and SN = 13-v, Table 4. These systems consist of 2 hydrogens and SN = 7 and SN = 7-v, respectively. Two different charge transfer behaviors were obtained in the SN = 13 ($PdPt_{12}(1)$ core–shell system + 2H) and in the system number 13-v ($PdPt_{12}(2)$ non-core shell-type +2H). In the first one of these, charge transfer of the Pd-core ($+0.28e^-$) and charge transfer of the hydrogens ($+0.05e^-$) to the $Pt_{12}(1)$-shell ($-0.33e^-$) was observed. This indicates that there is a charge transfer from the hydrogens to the core–shell structure. In the second case (SN = 13-v), charge transfer from the $PdPt_{12}(2)$ cluster ($+0.03e^-$) to the hydrogens ($-0.03e^-$) was obtained. In the former systems, it should be emphasized that the structure of the systems is very important in terms of the charge transfer process, given a reduction in hydrogens, when considering the cluster type system.

In the case of the interaction between SN = 7 and GNS (SN = 17 in Table 4), there was charge transfer from the surface ($+0.1e^-$) to the $PdPt_{11}(1)$ cluster. Following interaction with hydrogens (system number 21), charge transfer from the (PtN_4V_2) surface ($0.03e^-$) and the $PdPt_{11}(1)$ cluster ($0.06e^-$), to the hydrogens ($-0.09e^-$) was calculated. Notably, this system presents the most hydrogen dissociation of any of the systems (2.28 Å).

3.3 Adsorption energies

As apparent in Table 5, there is hydrogen adsorption in all our systems $\Delta E < 0$. There is a correlation between non-dissociation and low hydrogen adsorption energies ($|\ \Delta(E)\ | = 0.63 - 0.87$ eV Table 5. SN = 8 is not considered), which may also relate to a very low hydrogen charge transfer ($\pm$ 0.00–0.01e^- Table 5).

Systems involved are SN = 9,12,18 and 20 in Table 5. At the time when charge transfer increases ($\pm$ 0.03–0.09e^- Table 5) with respect to systems without dissociation, hydrogen dissociation is observed and the hydrogen adsorption energies are higher with respect to non-dissociated systems $|\ \Delta(E)\ | = 1.25 - 1.74$ eV. Systems involved in hydrogen dissociation and high adsorption energies are SN = 10,11,13, 13-v, 19 and 21 in Table 5.

To compare our results, we take the Pd_{13} + 2H system with number 9 in Table 5. A binding energy of 0.63eV was observed. This energy is lower than the Kubas state of 0.88eV reported in reference [37]. In the former case, the interaction of molecular hydrogen and one Pd atom in a Kubas state was considered [37]. In the former case, hydrogen adsorption energy is affected by the size of the catalyst.

3.4 Magnetic properties

General ferromagnetic behavior is found in our systems, induced by the d-orbital contribution of the palladium and platinum ions in the core–shell and cluster structures (non-core shell-type structures). Non-dissociation and very low value of charge transfer appear to correlate generally with high magnetic moments (m) ($m = 4.78 - 7.91$) μ_B, Table 5. The systems involved are SN = 9,12,18 and 20 in Table 5. Charge transfer produces dissociation and low magnetic states ($m = 0.19 - 5.62$) μ_B compared to systems that lack dissociation. The transition metal ions (Pd,Pt) adsorbed on the N_4V_2 substrate do not present a large contribution to the magnetic moment compared to the ions in the catalysts. The nitrogen doped pyridinic systems N_4V_2 and N_4V_2+H_2 and molecular hydrogen H_2, present no magnetic moment, Tables 5 and 6. The first one of these has already been studied in reference [1].

However, it has been reported that other nitrogen doped (pyrrolic and pyridinic) systems with one vacancy are spin-polarised [1]. Our magnetic behavior can be compared to the results in references [2, 10], where the magnetic behavior of free Pd_{13} cluster is 6 μ_B and is reduced to 4 μ_B, when it is deposed on the pristine graphene layer, after adsorption of one hydrogen molecule quenches the moment of the cluster to 2 μ_B [2, 10]. The magnetic behavior of references [2, 10] can be compared to the Pd-Pd_{12} core–shell system (SN = 3) with a magnetic moment of 8.17 μ_B Table 6. It is clear that our magnetic moment exceeds that described in references [2, 10]. After deposition of SN = 3 on GNS (SN = 14 Table 6), the magnetic moment diminishes to 4.31 μ_B. After hydrogen adsorption (SN = 18), the magnetic moment increases to 4.78 μ_B Table 5. As apparent, a different qualitative magnetic behavior was found because of the nature of the substrate. Another different qualitative magnetic behavior was evident in system number 4 in Table 6. SN = 4 presents a magnetic moment of 3.40 μ_B. After deposition of the former system on GNS (SN = 15), the magnetic moment increases to $m = 3.70\ \mu_B$. Hydrogen adsorption of SN = 15 leads to system number 19 and the magnetic moment decreases to $m = 2.27\ \mu_B$. However we found results similar to those given in references [2, 10] in our SN = 6 with $m = 8.07\ \mu_B$ and SN = 7 with a magnetic moment of $m = 3.81\ \mu_B$. After deposition of the former systems on GNS, the following magnetic moments were obtained $m = 5.30\ \mu_B$ (SN = 16) and $m = 3.63\ \mu_B$ (SN = 17), respectively. Finally, hydrogen adsorption of SN = 16 and SN = 17 diminishes the magnetic moment to $m = 5.06\ \mu_B$ (SN = 20) and 0.19 μ_B (SN = 21), respectively Tables 5 and 6.

3.5 Electronic properties

Metallic behavior (see Density of States (DOS) and d orbital Projected Density of States (PDOS) in Figures $\mathcal{S}3$–6 in the SI) and 3 main regions were identified in all our systems. The first one of these corresponds approximately to the structural bonding denoted by the hybridization of p_x, p_y and s orbitals of the C and N ions in the region $-20\ \text{eV} \lesssim E \lesssim -10\ \text{eV}$. The second one of these, $-10\ \text{eV} \lesssim E \lesssim -4\ \text{eV}$ is indicated by the hybridization of p_x, p_y, p_z and s orbitals of C and N ions and all d and s orbitals of Pd and Pt ions. The third region $-4\ \text{eV} \lesssim E \lesssim \varepsilon_F$ (ε_F being the energy of Fermi), is caused by the hybridization of p_z orbitals of C and N ions and all d and s orbitals of Pd and Pt. Generally, it is apparent that an s hydrogen orbital contribution occurs at around ε_F, when a hydrogen molecule is adsorbed on all systems. For system number 14 in Table 6, two different spin-dependent d-orbital contributions were found around $\varepsilon_F = -1.05$ eV. The first one consisted of d_{xz} and d_{xy} orbitals and the second one of $d_{x^2-y^2}$ orbitals of Pd. In the former system, the Pd-core orbital main contribution around Fermi's energy is caused by d_{xz} for both spins. In the case of SN = 16 in Table 6, two different spin-dependent d-orbital contributions were found at around $\varepsilon_F = -1.03$ eV. The first one consisted of d_{xy} and $d_{x^2-y^2}$ orbitals and the second one of $d_{x^2-y^2}$, d_{z^2}, d_{xy} and d_{xz}. The main contribution of the Pt-core orbital in this system is produced by d_{xy} and d_{yz} for one spin contribution and d_{xz} for the other. For the SN = 15, d_{z^2} orbitals of the Pt ion mainly hybridize with p_z orbitals for both spin polarizations around $\varepsilon_F = -1.17$ eV. In the case of SN = 17 in Table 6, two different spin-dependent d-orbital contributions were found around Fermi's energy $\varepsilon_F = -1.12$ eV for similar Pt and Pd ion contributions. The first of these basically consisted of entirely d-orbitals and the second of $d_{x^2-y^2}$ ones. Additionally, PDOS showed that there is no important contribution concerning Fermi's energy of the transition metal (Pd,Pt) ions adsorbed on the N_4V_2 substrate. Conversely, the main electronic contribution of the former ions is found in the first and second regions, which are the main regions that form the electronic structure of the surface.

4 Conclusions

In this work, a hydrogen adsorption study concerning graphene-based surfaces with core–shell type catalysts, using density functional theory is presented. A correlation between charge transfer and structural properties, hydrogen adsorption energies, magnetic behavior and electronic properties was found. A slab model composed of a pyridinic N_4V_2 system and an ensemble of hydrogen ions and initially Pd-Pd_{12}, Pt-Pt_{12}, Pd-Pt_{12} and Pt-Pd_{12} core–shells as catalysts was studied. In this work, Reduction of hydrogen, together with larger values of charge transfer for the highest values of hydrogen dissociation, compared to the case of non-dissociation was observed. Importantly in most cases, these values may be an order of magnitude greater, if compared to non-hydrogen dissociation behavior. For example, in this study, hydrogen charge transfer values for hydrogen dissociation ± (0.03–0.09) e^- are greater than the non-hydrogen dissociation case ± (0.00–0.01) e^-. Hydrogen dissociation is also related to oxidation of the (PtN_4V_2) surface. Hydrogen dissociation correlates with a non-core, shell-type structure, high adsorption energies and generally, low magnetic moments. Contrarily, non-hydrogen dissociation is directly related to low values (compared to the hydrogen dissociation case) of hydrogen charge transfer and to a reduction of the (PdN_4V_2) surface. In the same way non-hydrogen dissociation correlates with a core, shell-type structure, low hydrogen adsorption energies and high magnetic moments. Structural characterization indicates that structures with lower energies than those corresponding to the Pt-Pt_{12} and Pd-Pt_{12} core–shell ones were found for the gas phase and

on substrate. After optimization, the (Pd)Pt-core ions were found outside the cluster in the Pt-shell. It was also found that when the catalysts interact with initially N_4V_2 substrate, one transition metal ion is detached from the cluster to the substrate, changing the physical properties of the substrate. As is generally noted, the effect of the substrate on Pd(Pt)-Pd core–shell system increases the core–shell distance and decreases the distance between first neighboring ions inside the shell. Charge transfer for the non-hydrogen dissociation case involves core shell-type structures and presents two different charge transfer behaviors, which depend on the nature of the core ion and its electronegativity. In presence of surface oxidation of the core, in the case that the core is palladium and reduction in the case that it is platinum, the effect of hydrogen adsorption is to decrease the reduction of the surface in the non-hydrogen dissociation case. Contrarily, the effect of hydrogen adsorption is to decrease oxidation of the surface in the hydrogen dissociation case. Ferromagnetic behavior is found in our systems given by d-orbital contribution of the palladium and platinum ions in the catalysts. As mentioned previously the magnetic moment of our systems relates to hydrogen dissociation and charge transfer behavior. Metallic behavior and 3 main PDOS regions were identified in all our systems, produced by varying orbital hybridization. In contrast, very different d-orbital contribution was found in all our systems around Fermi's energy. In general, an s hydrogen orbital contribution is observed around Fermi's energy when hydrogen molecule is adsorbed on all systems. The importance of charge transfer in hydrogen dissociation suggested in this work may lead to further theoretical and experimental work and could be important for storing hydrogen. Besides, this study may also represent the first step for a subsequent theoretical study that involves larger clusters, where the core–shell interface plays an important role, as shown experimentally in reference [43].

Supplementary Information The online version contains supplementary material available at https://doi.org/10.1007/s42823-023-00463-w.

Declarations

Competing interests Author declares non-financial interests that are directly or indirectly related to the work submitted for publication.

References

1. Rangel E, Sansores E, Vallejo E, Hernández-Hernández A, López-Pérez PA (2016) Study of the interplay between N-graphene defects and small Pd clusters for enhanced hydrogen storage via a spill-over mechanism. Phys Chem Chem Phys 18(48):33158–33170. https://doi.org/10.1039/C6CP06497C
2. López MJ, Blanco-Rey M, Juaristi JI, Alducin M, Alonso JA (2017) Manipulating the magnetic moment of palladium clusters by adsorption and dissociation of molecular hydrogen. J Phys Chem C 121(38):20756–20762. https://doi.org/10.1021/acs.jpcc.7b03996
3. Luhadiya N, Kundalwal SI, Sahu SK (2021) Investigation of hydrogen adsorption behavior of graphene under varied conditions using a novel energy-centered method. Carbon Lett 31:655–666. https://doi.org/10.1007/s42823-021-00236-3
4. Kag D, Luhadiya N, Patil ND, Kundalwal SI (2021) Strain and defect engineering of graphene for hydrogen storage via atomistic modelling. Int J Hydrogen Energy 46(43):22599–22610. https://doi.org/10.1016/j.ijhydene.2021.04.098
5. Luhadiya N, Kundalwal SI, Sahu SK (2022) Adsorption and desorption behavior of titanium-decorated polycrystalline graphene toward hydrogen storage: a molecular dynamics study. Appl Phys A 128(49):1–13. https://doi.org/10.1007/s00339-021-05194-1
6. Gerber IC, Serp P (2020) A theory/experience description of support effects in carbon-supported catalysts. Chem Rev 120(2):1250–1349. https://doi.org/10.1021/acs.chemrev.9b00209
7. Psofogiannakis GM, Froudakis GE (2011) Fundamental studies and perceptions on the spillover mechanism for hydrogen storage. Chem Commun 47(28):7933–7943. https://doi.org/10.1039/C1CC11389E
8. Juarez-Mosqueda R, Mavrandonakis A, Kuc AB, Pettersson LGM, Heine T (2015) Theoretical analysis of hydrogen spillover mechanism on carbon nanotubes. Front Chem 3:2. https://doi.org/10.3389/fchem.2015.00002
9. Psofogiannakis GM, Froudakis GE (2009) DFT study of hydrogen storage by spillover on graphite with oxygen surface groups. J Am Chem Soc 131(42):15133–15135. https://doi.org/10.1021/ja906159p
10. Blanco-Rey M, Juaristi JI, Alducin M, López MJ, Alonso JA (2016) Is spillover relevant for hydrogen adsorption and storage in porous carbons doped with palladium nanoparticles? J Phys Chem C 120(31):17357–17364. https://doi.org/10.1021/acs.jpcc.6b04006
11. D'Anna V, Duca D, Ferrante F, Manna GL (2009) DFT studies on catalytic properties of isolated and carbon nanotube supported Pd_9 cluster-1: adsorption, fragmentation and diffusion of hydrogen. Phys Chem Chem Phys 11(20):4077–4083. https://doi.org/10.1039/B820707K
12. Alonso JA, López MJ (2018) Handbook of materials modeling: applications: current and emerging materials. Springer, New York
13. Rangel E, Sansores E (2014) Theoretical study of hydrogen adsorption on nitrogen doped graphene decorated with palladium clusters. Int J Hydrogen Energy 39(12):6558–6566. https://doi.org/10.1016/j.ijhydene.2014.02.062
14. Ma L, Zhang J-M, Xu K-W (2014) Hydrogen storage on nitrogen induced defects in palladium-decorated graphene: a first- principles study. Appl Surf Sci 292:921–927. https://doi.org/10.1016/j.apsusc.2013.12.080
15. Ma L, Zhang J-M, Xu K-W, Ji V (2015) Hydrogen adsorption and storage on palladium-decorated graphene with boron dopants and vacancy defects: A first-principles study. Phys E Low Dimens Syst Nanostruct 66:40–47. https://doi.org/10.1016/j.physe.2014.09.022
16. Faye O, Szpunar JA, Szpunar B, Beye AC (2017) Hydrogen adsorption and storage on palladium-functionalized graphene with NH-dopant: a first principles calculation. Appl Surf Sci 392:362–374. https://doi.org/10.1016/j.apsusc.2016.09.032
17. Ramos-Castillo CM, Reveles JU, Zope RR, de Coss R (2015) Palladium clusters supported on graphene monovacancies for hydrogen storage. J Phys Chem C 119(15):8402–8409. https://doi.org/10.1021/acs.jpcc.5b02358
18. Zhou Q, Wang C, Fu Z, Yuan L et al (2015) Hydrogen adsorption on palladium anchored defected graphene with B-doping: a theoretical study. Int J Hydrogen Energy 40(6):2473–2483. https://doi.org/10.1016/j.ijhydene.2014.12.071

19. Pašti IA, Jovanović A, Dobrota AS, Mentus SV et al (2018) Atomic adsorption on graphene with a single vacancy: systematic DFT study through the periodic table of elements. Phys Chem Chem Phys 20(2):858–865. https://doi.org/10.1039/C7CP07542A
20. Arrigo R, Schuster ME, Xie Z, Yi Y et al (2015) Nature of the N–Pd Interaction in Nitrogen–Doped carbon nanotube catalysts. ACS Catal 5(5):2740–2753. https://doi.org/10.1021/acscatal.5b00094
21. Yumura T, Kimura K, Kobayashi H, Tanaka R et al (2009) The use of nanometer-sized hydrographene species for support material for fuel cell electrode catalysts: a theoretical proposal. Phys Chem Chem Phys 11(37):8275–8284. https://doi.org/10.1039/B905866D
22. Prins R (2012) Hydrogen spillover. Facts and fiction. Chem Rev 112(5):2714–2738. https://doi.org/10.1021/cr200346z
23. Conner WC, Falconer JL (1995) Spillover in heterogeneous catalysis. Chem Rev 95(3):759–788. https://doi.org/10.1021/cr00035a014
24. Medenbach L, Köwitsch N, Armbrüster M et al (2018) Sulfur Spillover on Carbon Materials and Possible Impacts on Metal–Sulfur Batteries. Angew Chem Int Ed 57(41):13666–13670. https://doi.org/10.1002/anie.201807295
25. Psofogiannakis GM, Froudakis GE (2009) DFT study of the hydrogen spillover mechanism on Pt-doped graphite. J Phys Chem C 113(33):14908–14915. https://doi.org/10.1021/jp902987s
26. Wu HY, Fan X, Kuo JL, Deng WQ (2011) DFT study of hydrogen storage by spillover on graphene with boron substitution. J Phys Chem C 115(18):9241–9249. https://doi.org/10.1021/jp200038b
27. Kresse G, Hafner J (1993) Ab initio molecular dynamics for liquid metals. Phys Rev B 47(1):558–561. https://doi.org/10.1103/physrevb.47.558
28. Kresse G, Furthmüller J (1996) Efficient iterative schemes for ab initio total-energy calculations using a plane-wave basis set. Phys Rev B 54(1):11169. https://doi.org/10.1103/PhysRevB.54.11169
29. Blöchl PE (1994) Projector augmented-wave method. Phys Rev B 50:17953. https://doi.org/10.1103/PhysRevB.50.17953
30. Kresse G, Joubert D (1999) From ultrasoft pseudopotentials to the projector augmented-wave method. Phys Rev B 59:1758. https://doi.org/10.1103/PhysRevB.59.1758
31. Perdew JP, Burke K, Ernzerhof M (1996) Generalized gradient approximation made simple. Phys Rev Lett 77(18):3865–3868. https://doi.org/10.1103/PhysRevLett.77.3865
32. Deng D, Pan X, Yu L, Cui Y et al (2011) Toward N-doped graphene via solvothermal synthesis. Chem Mater 23(5):1188–1193. https://doi.org/10.1021/cm102666r
33. Parambhath VB, Nagar R, Ramaprabhu S (2012) Effect of nitrogen doping on hydrogen storage capacity of palladium decorated graphene. Langmuir 28(20):7826–7833. https://doi.org/10.1021/la301232r
34. Cardozo-Mata VA, Pescado-Rojas JA, Hernández-Hernández A, Hernández-Hernández LA et al (2020) Chemical interaction between nitrogen-doped graphene defects and a copper (1 1 1) surface: effects on water molecule adsorption. Appl Surf Sci 502(144149):1–8. https://doi.org/10.1016/j.apsusc.2019.144149
35. Kokalj A (1999) XCrySDen-a new program for displaying crystalline structures and electron densities. J Mol Graph Model 17:176–179. https://doi.org/10.1016/S1093-3263(99)00028-5
36. Cabria I, López MJ, Fraile S, Alonso JA (2012) Adsorption and dissociation of molecular hydrogen on palladium clusters supported on graphene. J Phys Chem C 116:21179–21189. https://doi.org/10.1021/jp305635w
37. Javan MB, Shirdel-Havar AH, Soltani A, Pourarian F (2016) Adsorption and dissociation of H_2 on Pd doped graphene-like SiC sheet. Int J Hydrogen Energy 41:22886–22898. https://doi.org/10.1016/j.ijhydene.2016.09.081
38. Vallejo E, López-Pérez PA (2022) Strong chemical adsorption of CO_2 and N_2 on a five-vacancy graphene surface. Solid State Commun. https://doi.org/10.1016/j.ssc.2022.114934
39. Zhao Y, Kim YH, Dillon AC, Heben MJ, Zhang SB (2005) Hydrogen storage in novel organometallic buckyballs. Phys Rev Lett 94(15):155504. https://doi.org/10.1103/physrevlett.94.155504
40. Song N, Wang Y, Zheng Y, Zhang J et al (2015) New template for Li and Ca decoration and hydrogen adsorption on graphene-like SiC: a first-principles study. Comput Mater Sci 99:150–155. https://doi.org/10.1016/j.commatsci.2014.12.016
41. Anderson RM, Zhang L, Loussaert JA, Frenkel AI, Henkelman G, Crooks RM (2013) An experimental and theoretical investigation of the inversion of Pd@Pt core@shell dendrimer-encapsulated nanoparticles. ACS Nano 7(10):9345–9353. https://doi.org/10.1021/nn4040348
42. Karim W, Spreafico C, Kleibert A, Gobrecht J et al (2017) Catalyst support effects on hydrogen spillover. Nature 541:68–71. https://doi.org/10.1038/nature20782
43. Kobayashi H, Yamauchi M, Kitagawa H, Kubota Y, Kato K, Takata M (2008) Hydrogen absorption in the core/shell interface of Pd/Pt nanoparticles. J Am Chem Soc 130(6):1818–1819. https://doi.org/10.1021/ja078126k